The Use of *In Situ* X-Ray Diffraction, Optical Scattering and Resistance Analysis Techniques For Evaluation of Copper Diffusion Barriers in Blanket Films and Damascene Structures

C. Cabral, Jr., C. Lavoie, J.M.E. Harper, and J.L. Jordan-Sweet
IBM T.J. Watson Research Center, Yorktown Heights, NY 10598

Copper wiring is quickly becoming the choice in the semiconductor industry to replace aluminum wiring[1]. As the industry approaches the 0.1 μm linewidth generation of chips copper will allow for improved electromigration resistance[2] and thus reliability, as well as improved conductivity[3]. Copper has been most widely integrated using a dual damascene[4] and electroplated deposition[5] approach. One concern is that Cu easily diffuses through dielectrics and will act as a deep-level trap in Si[6], degrading the performance of CMOS transistors. It is therefore important to have a thin diffusion barrier[7] between Cu and the dielectric. In the published literature there have been many papers discussing barriers that are thermally stable and have good conductivity, such as Ta[8-12], TiW[8], TaSiN[13-15] and TiN[8,11,16]. The techniques used to determine the effectiveness of Cu diffusion barriers have generally been employed *ex situ,* after the structure has been annealed. Electrical techniques such as capacitance-voltage measurements, diode measurements and sheet resistance measurements, along with electron and x-ray diffraction, and Auger, RBS and SIMS analysis are some of the ways barrier failure has been determined. Instead of this rather slow evaluation process, we describe here the use of three different *in situ* techniques, employed simultaneously, to determine Cu diffusion barrier failure temperatures. *In situ* x-ray diffraction, optical scattering and sheet resistance analysis as a function of temperature are used to rapidly evaluate Ta, Ti_3W_{97}, $Ta_{36}Si_{12}N_{52}$ and TiN barriers between Cu and Si.

Copper diffusion barrier films, 21 to 24 nm thick, were deposited in two different magnetron sputtering systems. The $Ta_{36}Si_{12}N_{52}$ films were reactively (N_2 and Ar plasma) co-sputtered from Ta and Si targets in an ultra high vacuum deposition system. The Ta, TiN and Ti_7W_{93} films were deposited in a high vacuum, MRC 643, side scan system from planar targets. The TiN film was reactively deposited and the Ti_7W_{93} film was deposited from a W(10 at.% Ti) alloy target. A 200 nm Cu layer was deposited on top of the various barrier layers, without breaking vacuum.

The diffusion barrier films described above were deposited either as blanket films on Si substrates or in patterned damascene features. The blanket films deposited on single crystal Si were evaluated with *in situ* x-ray diffraction and optical scattering analysis, whereas those deposited on 150 nm polycrystalline-Si were evaluated with the additional technique of *in situ* sheet resistance analysis. Submicron damascene features were formed using x-ray lithography together with standard Si processing techniques. The resulting structures had 0.6 μm SiO_2 / Si sidewalls and Si(100) bottoms with widths ranging from 0.23 to 0.62 μm (aspect ratios 0.97 to 2.6) and lengths from 5.1 to 80 μm. The incident x-ray and laser spot size on the patterned features encompassed one half to one million damascene structures.

Copper diffusion barrier failure was studied in blanket films and damascene features, described above, using three different *in situ* techniques (Fig. 1), conducted simultaneously, while the samples were annealed in nitrogen at a temperature ramp rate of 3 °C/s from 100 to 1000 °C. The analysis was completed at the National Synchrotron Light Source, Brookhaven National Laboratory on beamline X20C[17]. A schematic of the x-ray diffraction technique is depicted in Fig. 1a. An incident x-ray beam which passed through a wide-bandpass, artificial multilayer monochromator gave an

energy resolution of 1.5% at 6.9 keV (λ = 0.1797 nm) with an average flux of 3 X 10^{12} photon/s. A set of beam defining slits provided an incident x-ray spot size of 2X2 mm on the sample surface. As the samples were annealed, the diffracted x-ray intensity was monitored using a linear, position sensitive detector. The detector covered a two theta range from 46 to 56°, from which data was collected every 0.5 s (1.5 °C). The range was chosen such that the Cu(111) and Cu silicide reflections could be simultaneously monitored. Temperature was monitored using a k-type thermocouple, which was calibrated using eutectic melting points of various metals in contact with Si for an accuracy of +/- 3 °C.

The second *in situ* technique, optical scattering, is depicted in Fig. 1b. A chopped HeNe laser beam is brought into the annealing chamber through a fiber optic cable and is then focused through a lens onto the sample surface at an incidence angle of 65°, forming a spot size of 1X2 mm. The scattered intensities are measured using two bare fibers positioned at 50° and -21°, allowing for measurement of lateral length scales of 5 and 0.5 μm, respectively. For detection of only the chopped HeNe light scattered from the sample surface, lock-in amplifiers are used with Si photodiodes and interference filters, which remove background light at other wavelengths. With the optical scattering technique, not only surface roughness changes but also changes in index of refraction that barrier failure may cause (coexistence of multiple phase/composition domains), will lead to changes in the scattered intensity.

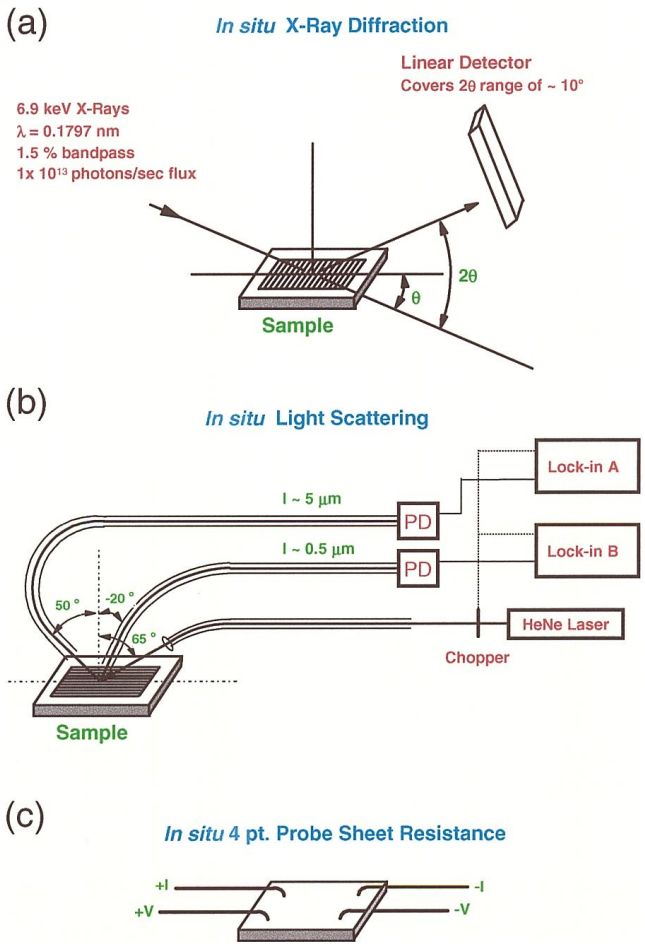

Figure 1. Schematic representations of the analysis techniques used to evaluate copper diffusion barriers. The techniques include (a) in situ *x-ray diffraction, (b)* in situ *optical scattering and (c)* in situ *sheet resistance analysis.*

The last *in situ* technique used, Fig.1c, is a four-point probe sheet resistance measurement as a function of temperature. Four spring-loaded Ta probes arranged approximately in a square geometry maintain contact with the sample surface, while 25 mA of current pass through two of the probes, and voltage is measured across the other two. This allows for a relative sheet resistance measurement that is scaled using a room temperature, absolute measurement made with a fixed in-line four-point probe geometry.

The method used for determining the Cu diffusion barrier failure temperatures from the *in situ* x-ray diffraction analysis is shown in Fig. 2. For this example a Ta barrier layer between Cu and poly-Si is annealed. The x-ray detector is placed such that the Cu(111) and Cu silicide reflections are present in the selected two-theta range. This two-theta range, from 48 to 54°, is plotted as a function of the annealing temperature (Fig. 2a), where contours and color indicate the diffracted x-ray intensity. Low intensity is indicated by blue shading and higher intensity is indicated by red shading. As is evident from the plot, the Cu(111) peak starts decreasing in intensity at about 720 °C as the Cu silicide peak grows in intensity. In order to determine the barrier failure temperature, two-theta ranges are taken around each x-ray reflection, as indicated by the white lines. Figure 2b represents a plot of the summed logarithm of x-ray intensity as a function of temperature for both the Cu(111) and Cu silicide two-theta ranges. Again, it is evident that at about 720 °C the Ta barrier starts to fail and that the midpoint in the failure occurs at about 732 °C. The final step for determination of a failure temperature consists of taking the derivatives, maximum change in x-ray intensity, of the curves in Fig. 2b. The derivatives of the Cu(111) and Cu silicide integrated x-ray intensity curves as a function of temperature are shown in Fig. 2c. The temperature at which maxima (Cu(111)) and minima (Cu silicide) occur in the derivative curves allow us to compare failure between barrier types and underlying structures. For the Ta barrier, as indicated by this method, failure occurs at 728 and 735 °C for the appearance of the Cu silicide reflection and disappearance of the Cu(111) reflection, respectively.

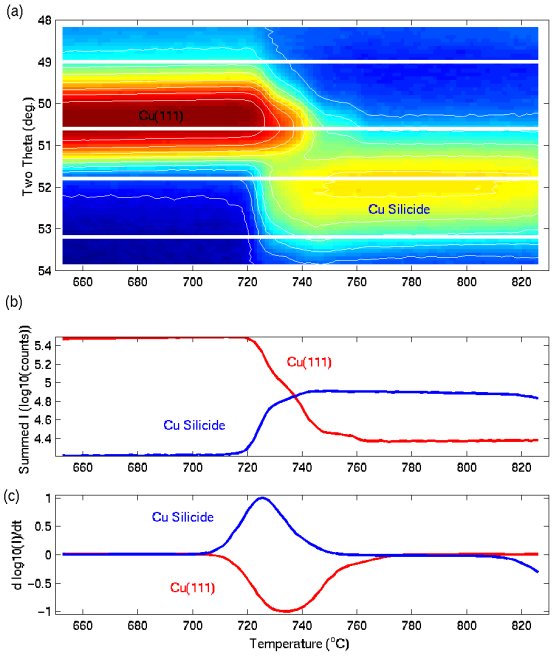

Figure 2. In situ *x-ray diffraction showing diffusion barrier failure for a blanket tantalum thin film between copper and polycrystalline silicon. The film was annealed at 3 °C/s from 100 to 1000 °C in nitrogen. The plots show (a) x-ray intensity as a function of two-theta angle and temperature, (b) summed x-ray intensity as a function of temperature and (c) the derivative of summed x-ray intensity as a function of temperature.*

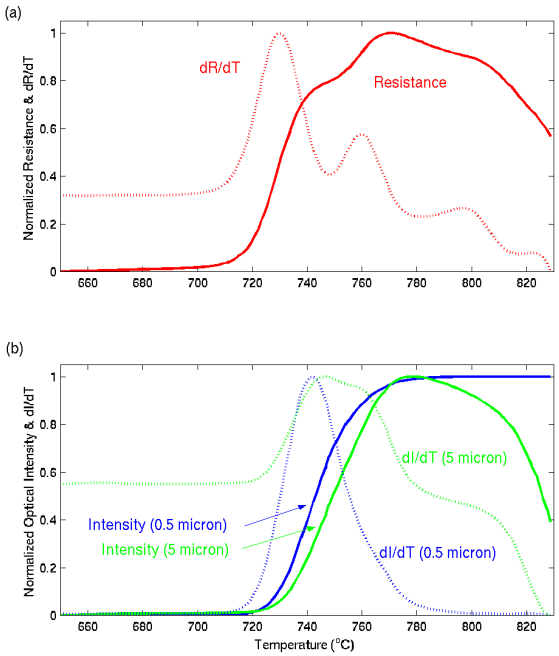

Figure 3. This figure shows (a) in situ *sheet resistance analysis as a function of temperature and (b)* in situ *optical scattering as a function of temperature at two different length scales (0.5 and 5 μm). The analysis was conducted simultaneously with the x-ray diffraction analysis (Fig. 2). The respective derivatives are shown as dashed curves on the plots.*

The analysis methods used to determine barrier failure with the *in situ* techniques of optical scattering and sheet resistance are depicted in Fig. 3. This analysis was conducted simultaneously with x-ray diffraction analysis shown in Fig. 2 for a blanket Ta barrier on poly-Si. Normalized sheet resistance as a function of temperature is shown in Fig. 3a (solid curve) where a deviation from the typical linear behavior for a metal film starts to occur at about 710 °C indicating the start of barrier failure. Also plotted (dashed curve) is the derivative of the sheet resistance as a function of temperature. The first and highest maxima indicates the temperature at which the maximum resistance increase has occurred and is recorded as the barrier failure temperature (729 °C). Elastic light scattering as a function of temperature is shown in Fig. 3b (solid curves) for two different lateral length scales, 0.5 and 5 μm. The intensities for both length scales start to increase at about 720 °C indicating changes in surface roughness and/or index of refraction due to barrier failure. The derivatives of the optical curves are plotted (dashed curves) and again the maxima are recorded as the failure temperatures. The failure temperatures from the optical analysis are 742 and 747 °C for the 0.5 and 5 μm length scales, respectively.

The barrier failure temperatures found by the three *in situ* techniques correlate well, as shown in Table 1. The table is divided into failure temperatures determined on blanket films (on the left) versus patterned damascene features (on the right). The blanket film category is further divided into failure on poly-Si versus Si(100). For the failure temperatures as determined by x-ray diffraction the temperatures for the Cu(111) peak disappearance and Cu silicide peak appearance are averaged together, and likewise for the optical scattering the failure temperatures found with both length scales are averaged together. Concentrating on the left side of the table the average standard deviation in barrier failure temperatures between the x-ray, resistance, and optical techniques on poly-Si is 10 °C and that on Si(100) (no resistance analysis) is 11 °C. The average difference between x-ray and optical techniques for the patterned damascene structures is 3 °C (temperature measurement error in all cases +/- 3 °C).

The trends in barrier failure as a function of line length and aspect ratio in the damascene features are shown in Fig.4. The features analyzed for Fig. 4b varied in linelength but had a constant linewidth of 0.33 μm and aspect ratio of 1.8. The plot indicates that the barrier failure temperatures are independent of the

length. When the failure temperatures are plotted (Fig. 4a) as a function of aspect ratio (linewidth 0.23 to 0.62 μm) it becomes clear that as the aspect ratio is increased (linewidth decreased) the barrier failure temperatures decrease. This trend is consistent for all the barriers except the TiN, which shows an increase in failure temperature at the largest aspect ratio. At the higher aspect ratios it is expected that with the conventional magnetron sputtering process, used to deposit the barriers, the coverage on the damascene structures sidewalls and corners will decrease, causing lower barrier failure temperatures, as observed.

In summary, three different *in situ* techniques, x-ray diffraction, optical scattering, and sheet resistance analysis, measured as a function of temperature, are all effective in the rapid determination of Cu diffusion barrier failure temperatures. From this work, it was found that the order of increasing effectiveness of the Cu diffusion barriers studied is Ta <Ti_7W_{93} < $Ta_{36}Si_{12}N_{52}$ < TiN. It was also shown that when the barriers were used in damascene structures the barrier failure temperature was independent of the damascene structure length, but did depend on the aspect ratio (structure width). For all barriers except TiN, the diffusion barrier failure temperature decreased with increasing aspect ratio (decreasing structure width).

Acknowledgments

The authors would like to thank the staff of the IBM Advanced Lithography Facility and Silicon Innovation Facility, R. Carruthers for film deposition and G. Coleman for Rutherford Backscattering Spectroscopy. The work was completed at the National Synchrotron Light Source, Brookhaven National Laboratory under DOE contract DE-AC02-76CH-00016.

References

[1] D. Edelstein, J. Heidenreich, R. Goldblatt, W. Cote, C. Uzoh, N. Lustig, P. Roper, T. McDevitt, W. Motsiff, A. Simon, A. Stamper, J, Dukovic, R. Wachnik, H. Rathore, S. Luce, and J. Slattery, IEDM Tech. Digest, 773 (1997).

[2] S. Venkatesan, A.V. Gelatos, V. Misra, R. Islam, B. Smith, J. Cope, B. Wilson, D. Tuttle, R. Cardwell, I. Yang, P.V. Gilbert, R. Woodruff, R. Bajaj, S. Das, J. Farkas, D. Watts, C. King, P. Crabtree, T. Sparks, T. Lii, C. Simpson, A. Jain, M. Herrick, C. Capasso, S. Anderson, R. Venkatraman, S. Filipiak, B. Fiordalice, K. Reid, J. Klein, E.J. Weitzman, and H. Kawasaki, IEDM Tech. Digest, 769 (1997).

[3] C.-K. Hu, K.Y. Lee, L. Gignac, S.M. Rossnagel, C. Uzoh, K. Chan, P. Roper, and J.M.E. Harper, Mat. Res. Soc. **514**, 287 (1998).

[4] M.M. Chow, W.L. Guthrie, J.E. Cronin, C.W. Kanta, B. Luther, K.A. Perry, and C.L. Stanley, U.S. Patent 4,789,648, (1988).

[5] P.C. Andricacos, Interface **7(1)**, 23 (1998).

[6] S.M. Sze, *Semiconmductor Devices, Physics and Technology* (Wiley, New York, 1985).

[7] M.-A. Nicolet, Defect and Diffusion Forum **143-147**, 1271 (1997).

[8] C.-K. Hu, S. Chang, M.B. Small, and J.E. Lewis, VMIC Conf., 181 (1986).

[9] K. Holloway, P.M. Fryer, C. Cabral, Jr., J.M.E. Harper, P.J. Bailey, and K.H. Kelleher, J. Appl. Phys. **71**, 5433 (1992).

[10] L.A. Clevenger, N.A. Bojarczuk, K. Holloway, J.M.E Harper, C. Cabral, Jr., R.G. Schad, F. Cardone, and L. Stolt, J. Appl. Phys. **73(1)**, 300 (1993).

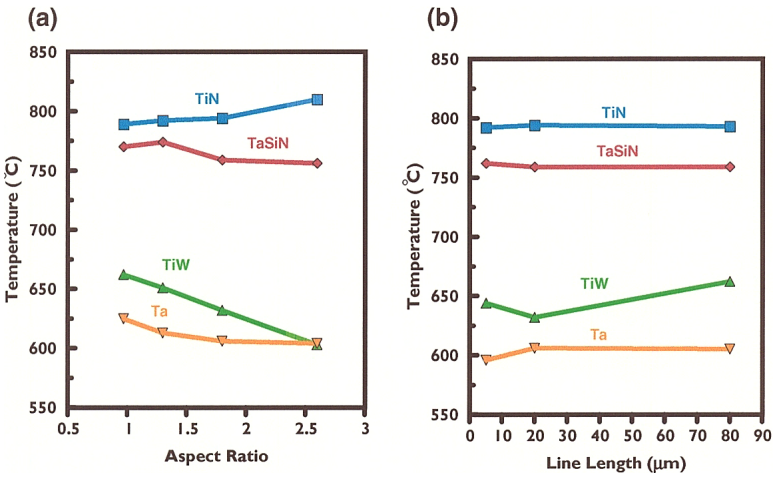

Figure 4. Barrier failure temperatures comparing Ta, TiW, TaSiN and TiN copper diffusion barriers in patterned damascene structures as a function of (a) aspect ratio and (b) structure length.

Table 1

	Blanket Films			Patterned Features	
PolySi/Si(100)	X-Ray (°C)	Optical (°C)	Resistance (°C)	X-Ray (°C)	Optical (°C)
Ta	732 / 722	742 / 731	729 / ---	610	601
Ta_7W_{93}	791 / 761	803 / 783	800 / ---	629	630
$Ta_{36}Si_{12}N_{52}$	829 / 807	862 / 779	850 / ---	759	764
TiN	940 / 815	920 / 821	923 / ---	813	816

[11] S. Simon Wong, C. Ryu, H. Lee, K.-W. Kwon, Mat. Res. Soc. Proc. 514, 75 (1998).
[12] M.T. Wang, Y.C. Lin, and M.C. Chen, J. Electrochem. Soc. **145(7)**, 2538 (1998).
[13] D.-J. Kim, Y.-T. Kim, J.-W. Park, J. Appl. Phys. **82(10)**, 4847 (1997).
[14] Y.-J. Lee, B.-S. Suh, S.-K. Rha, and C.-O. Park, Thin Solid Film **320**, 141 (1998).
[15] D. Fischer, T. Scherg, J.G. Baur, H.-J. Schulze, and C. Wenzel, Microelectronic Engineering **50**, 459 (2000).
[16] S.-K. Rha, S.-Y. Lee, W.-J. Lee, Y.-S. Hwang, C.-O. Park, D.-W. Kim, Y.-S. Lee, and C.-N. Whang, J. Vac. Sci. Technol. B **16(4)**, 2019 (1998).
[17] G.B. Stephenson, K.F. Ludwig, Jr., J.L. Jordan-Sweet, S. Brauer, J. Mainville, Y.S. Yang, and M. Sutton, Rev. Sci. Instrum. **60**, 1537 (1989).

Polymer Chain Relaxation: Surface Outpaces Bulk

W. E. Wallace[*], D. A. Fischer[*], K. Efimenko[†], W. L. Wu[*], and J. Genzer[†]
[*]National Institute of Standards and Technology, 100 Bureau Drive, Gaithersburg, MD
[†]North Carolina State University, Department of Chemical Engineering, Raleigh, NC

The time scale that controls polymer chain relaxation has taken on a new importance as the paradigm for polymer innovation evolves from three dimensions to two.[1] Nanotechnology initiatives, involving the design and fabrication of highly confined polymer layers, drive the need for a comprehensive description of chain dynamics, as bulk polymers become thinner and more surface-like. In this study we apply near-edge X-ray absorption fine structure (NEXAFS)[2,3] to measure directly both surface and bulk segmental relaxation throughout a uniformly deformed polystyrene slab. Using this methodology, in a single experiment, chain relaxation is found to occur almost 50% faster at the surface than in the bulk.

Rectangular samples (12.5 x 12.5 x 6 mm), prepared by vacuum hot-pressing at 150 °C monodisperse polystyrene (M_W = 228,000 g/mole), were placed into a steel channel die and uniaxially elongated at room temperature along one of the long dimensions to about 130% of their original length. This sample preparation allowed us to examine true bulk samples as encountered in practice and to avoid thin film effects that may alter the free surface behavior.[4] Partial electron yield (PEY, kinetic energy > 150 eV) and fluorescence yield (FY, carbon K_α 277 eV) carbon K-edge NEXAFS intensities, with probing depths of approximately 2 and 200 nm, respectively, were recorded simultaneously at the NIST/Dow Materials Characterization end-station (beamline U7A at the National Synchrotron Light Source, Brookhaven National Laboratory).[3] For each sample, PEY and FY were measured with the incident polarized X-ray beam normal to the sample surface and at two azimuthal sample orientations: with the electric field vector, **E**, parallel ($\phi = 0°$) and perpendicular ($\phi = 90°$) to the elongation direction as shown in Fig. 1.

Orientation of the chain backbone was determined by monitoring the C=C phenyl ring 1s $\rightarrow \pi_1^*$ NEXAFS resonance intensity at 285.5 eV,[3,5] which involves the excitation of carbon 1s electrons to the unfilled p* antibonding orbitals of the phenyl ring. Enhancement of the 1s $\rightarrow \pi_1^*$ resonance intensity was observed when **E** was parallel to the elongation direction. Since the phenyl π^* orbitals are oriented normal to the phenyl rings, and the phenyl rings, free to rotate around the pendant bond, will have a component normal to the chain axis, the intensity of the π^* signal has been shown to be an unambiguous signature of backbone orientation.[6] This orientation, seen both in the PEY and the FY NEXAFS signals of the elongated samples, provides clear evidence of chain orientation at the outset of the experiment. A direct measure of the chain relaxation rates at the surface and in the bulk can be obtained by defining an orientation factor, OF (see Figure 2 caption) that is evaluated from the time dependence of the 1s $\rightarrow \pi_1^*$ resonance intensity in the PEY (relative uncertainty ± 0.01%) and FY (relative uncertainty ± 0.05%) NEXAFS spectra, respectively, during annealing. Figure 2 shows that while the OF for both surface and bulk chains decays as a function of increasing annealing time at 60 °C,[7] the surface orientation is initially greater and decays faster than for the bulk. Fitting the decay rates to exponential functions gives characteristic time constants of approximately 33 and 50 minutes (with corresponding R^2 values of 0.90 and 0.91) for the surface and the bulk, respectively.

These results show conclusively that polystyrene surface chain relaxation dynamics are significantly faster than the bulk. Our results are in accord with recent theory predicting that collective motion on chain loops extended to the sample surface is responsible for a rapid increase of chain mobility near the surface

region of the film (top ≈ 5 nm).[8] The finding that the polystyrene surface segmental mobility greatly outpaces the bulk is expected to be a universal property of polymeric chains profoundly influencing the design, processing, and application of polymeric materials.

References

1. Jones, R.A.L. and Richards, R.W. *Polymers at Surfaces and Interfaces* (Cambridge University Press, Cambridge, 1999).
2. Stöhr, J. *NEXAFS Spectroscopy* (Springer-Verlag, Berlin, 1992).
3. Fischer, D.A., Mitchell, G.E., Yeh, A.T. & Gland, J.L. *Appl. Surf. Sci.* **133**, 58-64 (1998).
4. Schwab, A.D., Agra, D.M.G., Kim, J.H., Kumar, S. and Dhinojwala, A. *Macromolecules* **33**, 4903-4909 (2000).
5. Kikuma, J. and Tonner, B.P. *Journal of Electron Spectroscopy and Related Phenomena* **82**, 53-60 (1996).
6. Liu, Y., Russell, T.P.; Samant, M.G., Stöhr, J.; Brown, H. R.; Cossy-Favre, A. & Diaz, J. *Macromolecules* **30**, 7768-7771 (1997).
7. Kovacs, A.J. & Hobbs, S.Y. *Journal of Applied Polymer Science* **16**, 301-303 (1972).
8. de Gennes, P.G. *Eur. Phys. J E* **2**, 201-205 (2000); de Gennes, P.G., manuscript.

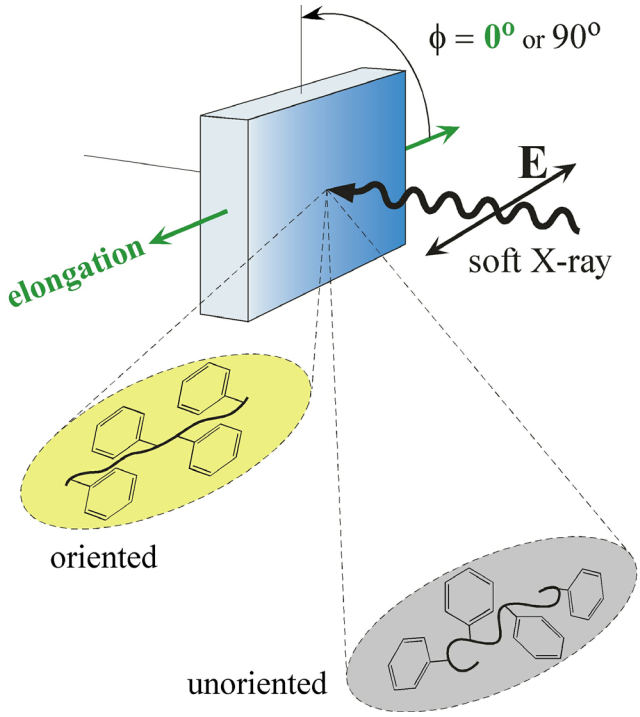

*Figure 1. The schematic details the sample geometry for the incident polarized soft X-ray beam normal to the polystyrene sample surface with the elongation direction parallel to **E** (ϕ = 0°). The insets represent chain configurations in oriented (before annealing) and unoriented (after annealing) elongated samples.*

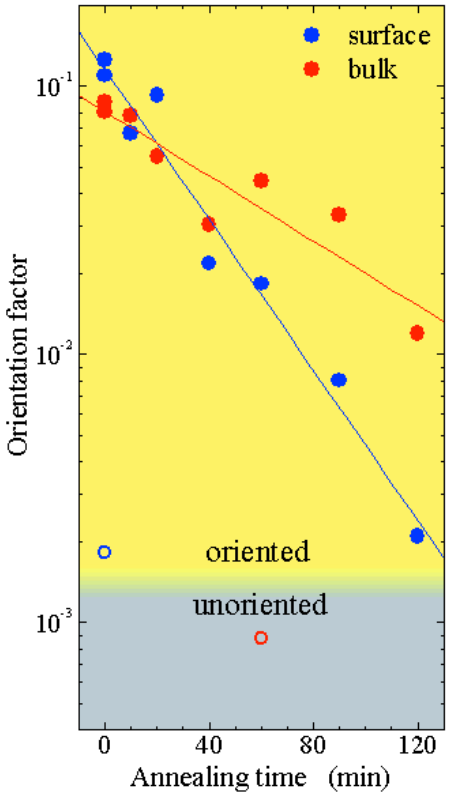

Figure 2. Time evolution of the orientation factor, OF, from an elongated (oriented) polystyrene sample reveals that when annealed at 60 °C the surface chains relax to an equilibrium (unoriented) configuration faster than the bulk chains. OF is calculated from $(I_{\parallel} - I_{\perp})/(I_{\parallel} + I_{\perp})$, where $I_{\parallel}$ and $I_{\perp}$ are the 1s → π_1 resonance NEXAFS intensities collected with the sample elongation direction parallel (ϕ = 0°) and perpendicular (ϕ = 90°) to the electric vector of the soft X-ray beam, **E**, respectively. The blue circles denote OF from the partial electron yield NEXAFS signal (surface region) and the red circles represent the fluorescence yield NEXAFS signal (bulk region), measured simultaneously. The closed and open circles depict OF evaluated from data collected on elongated specimens and those not subjected to elongation, respectively. The solid lines represent exponential decay fits to the experimental data on the elongated samples; the rate decay constants are reported in the text.*